https://doi.org/10.1016/j.asr.2019.01.033

Deformation Monitoring Using GNSS-R Technology

Yang Yang, Yu Zheng, Wenkun Yu, Wu Chen, Duojie Weng
Department of Land surveying and Geo-informatics
Hong Kong Polytechnic University

Abstract

GNSS reflectometry (GNSS-R) has been widely studied in recent years for various applications, such as soil moisture monitoring, biomass analysis, and sea state monitoring. This paper presents the concept of a novel application of using GNSS-R technology for deformation monitoring. Instead of installing GNSS on the deformation body to sense the movement, GNSS-R deformation monitoring system estimates the deformation from receiving GNSS reflected by the deformation body remotely. A prototype of GNSS-R deformation monitoring system has been developed based on GNSS software receiver technology. A 3D geometrical model of GNSS signal reflection has been used to reveal the relationship between the change of carrier phase difference and deformation. After compensating the propagation path delay changes caused by satellite movement, the changes in the remaining carrier phase difference are linked to the deformation. Field tests have been carried using the GNSS-R system developed and the results show sub-centimeter level deformation can be observed with the new technology. Unlike other GNSS deformation monitoring methods, GNSS-R receivers are not installed on the slope which makes this new technology more attractive.

Introduction

Global Navigation Satellite System Reflectometry (GNSS-R) has been first proposed in 1993 by Martin-Neira (1993), as a promising technique for altimetry application to receiving GNSS signals from a reflected surface. GNSS-R can be considered as a new type of remote sensing technology using GNSS signals as the resources, as some characteristics of GNSS signals will alter due to the reflection which are , related to the properties of the reflecting surfaces.

Various applications of GNSS-R have been developed and can be generally categorized into two groups: non-geometrical and geometrical methods. The non-geometrical methods are usually focusing on the amplitude or the power of the reflected signals. The applications of this type include the sea state monitoring (Soulat et al., 2004), biomass monitoring (Ferrazzoli et al., 2011), soil moisture monitoring (Egido et al., 2008), snow depth estimation (Jacobson, 2008), etc. The geometrical methods are focusing on the range difference of the direct and reflected signals. Depending on GNSS signal structure and application requirements, two types of altimetry algorithms have been proposed based on either code or carrier phase measurements. Due to the narrow bandwidth of code signals, the precision of code measurement is relatively lower. However, it possesses the advantage of the capability to provide range measurement over the rough or dynamic surface, like sea surface in windy weather. The precision of the several centimeters level in an average of a relatively long period of time (e.g. a few minutes) has been achieved using code altimetry (Lowe et al., 2002; Ruffini et al., 2004). An approach called interferometric GNSS-R (iGNSS-R) has been developed by taking the direct signal for correlation, instead of using locally generated code replica (Rius et al., 2012). The comparison results of both approaches have been studied by (Cardellach et al., 2014) in an airborne experiment, which show that the iGNSS-R is at least two times better in precision than the traditional approach. The carrier phase altimetry has been tested on various platforms over difference earth surfaces, i.e. lake surface monitoring from cliffs (Treuhaft et al., 2001) and from aircraft (Semmling et al., 2014), sea surface monitoring over bridges (Rivas and Martin-Neira, 2006) and sea ice monitoring by TechDemoSat-1 satellite (Li et al., 2017; Hu et al., 2017).

A new application of slope deformation monitoring has been inspired by the remarkable achievements of GNSS-R altimetry, the theory and the possible methods are proposed in this paper. The general definition of deformation is the change in shape or size of an object due to applied force or changing temperature. As to the engineering structure such as dams, slopes, bridges and buildings, the deformation also involves the change in spatial position and altitude. Engineering structures are subject to deformation due to the factor of ground water level, tidal phenomena, tectonic phenomena, etc.(Erol et al., 2004). Periodic monitoring of the structural response is necessary to rationally secure and maintain the safety of structures (Park et al., 2007). Normally, the deformation monitoring can be achieved by multiple techniques, for example conventional approaches (precise levelling, angle and distance measurement etc.), photogrammetric (aerial, satellite photogrammetry), positioning system (Global Position System) and radar system (InSAR), as well as some special techniques using laser ranger, tiltmeters, strainmeters etc. (Erol et al., 2004), depending on the surrounding environment and the budget. While developing the novel method of using GNSS-R for deformation monitoring possesses lots of advantages. The traditional method of deformation monitoring using GNSS needs to deploy multiple stations on the target surface. While by using reflected GNSS signal, the proposed method could monitor the target with single station at a distance of a few hundred meters away. This advantage is necessary when applying to the unreachable objects in case of emergency, e.g. in the sceanario to monitor a deforming slope surface that is dangrous to install equipment on. And it is also possible for multiple targets monitoring at same time considering there are dozens of GNSS satellites available on different directions nowadays. And comparing with the aerial, satellite photogrametry and InSAR system, the cost of the GNSS receiver is much lower, and the deployment could be much easier due to the simple system.

The traditional GNSS-R altimetry methods are not suitable to be applied to the deformation monitoring straightly. The deformation monitoring requires precise measurement result and relatively accurate spatial position of the monitoring object. And the environment might be complicated depending on the observation location and the target. To fulfill the requirements and meet the challenges, the carrier phase of the GNSS signal has drawn the attention due to its potential ability of precise measurement; the previous research of the application of GNSS-SAR (Zheng et al., 2017) has been employed for the spatial position determination; and a geometrical model has been applied to compensate the error caused by the environmental variation. By taking the GPS signal as an example, this paper demenstrats the theory, method, feasibility and accuracy of using GNSS-R technology for deformation monitoring.

The principle of using GNSS-R for deformation monitoring

The principle of using GNSS-R for slope deformation monitoring is to estimate the carrier phase differences from both direct and reflected signals, then retrieve the slope deformation from the carrier phase differences. The geometry of signal propagation is shown in figure 1. There are two different types of antenna involved: the right-hand circular polarization (RHCP) antenna for direct signal collection, and left-hand circular polarization (LHCP) antenna for reflected signal collection. Usually, the reflected signal power is much weaker due to the scattering. To ensure the signal tracking results are of acceptable quality, the receiver is normally placed not too far away (i.e. a few hundred meters, unless high gain directional antenna is used) from the monitoring surface for stronger signal strength.

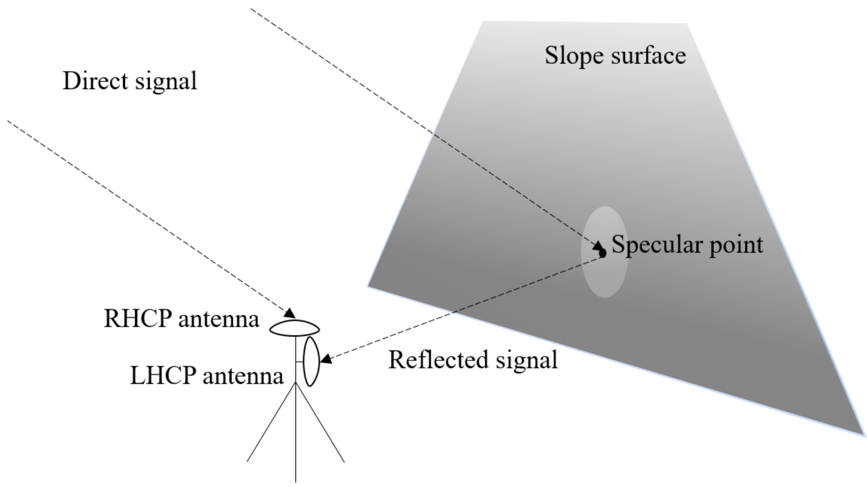

Figure 1. The geometry of using GNSS-R for slope deformation monitoring.

For GPS satellite, the transmitted signal of the L1 band can be expressed as:

$$T(t) = A_T \cdot cos(\omega t + \varphi_L)\, y(t) d(t) \tag{1}$$

Here, the term ωt represents the GPS signal carrier frequency. $\varphi_L$is the GPS signal carrier phase; $y(t)$ is the C/A code sequence; $d(t)$ is the GPS satellite navigation message.

When the signal arrives at the receiver, it can be expressed as the transmitted signal delayed by time τ and reduced in amplitude. The received direct signal can be expressed as:

$$R_d(t) = A_d \cdot cos((\omega + \omega_{Dd})(t - \tau_d) + \varphi_d)\, y(t - \tau_d) d(t - \tau_d) + n \tag{2}$$

where τ_d is the time delay for the signal travelling from the transmitter to the direct antenna; the term $\omega(t - \tau_d)$ represents the signal carrier frequency, and $\omega_{Dd}(t - \tau_d)$ represents the Doppler frequency caused by the relative movement between satellite and receiver; φ_d is the carrier phase of the received direct signal, which is corresponding to the signal transmitting time $t - \tau_d$; A_d is the amplitude of the direct signal when received; and n is the overall noise.

The transmitted signal reaches and is reflected off the object surface, the area of signal reflection is described using first Fresnel zone (calculation refers to Larson et al., 2010), shown as lighter color in figure 1. The location of sensed area can be detected by applying the GNSS-SAR technology. The reflected signal can be expressed as:

$$R_r(t) = A_r \cdot cos((\omega + \omega_{Dr})(t - \tau_r) + \varphi_r)\, y(t - \tau_r) d(t - \tau_r) + n \qquad (3)$$

Here, A_r represents the amplitude of the reflected signal, including all losses as same as the direct signal, plus the losses caused by extra propagation path and the surface scattering. The scattering loss may vary depending on the surface material and the roughness. τ_r is the time delay of the reflected signal regarding to the transmitted signal; φ_r is the reflected signal carrier phase; n is the overall noise. In this scenario, the navigation message $d(t)$ from the direct and reflected signal would be same, and the Doppler frequency difference would be negligible.

The range difference can be estimated if the direct and reflected signals are synchronized and steadily tracked. The carrier phase is chosen in this application for its potential ability of precise measurement. In a GNSS software receiver, the carrier phase measurement is estimated by the tracking loop. The received signal after amplification, down-conversion and analog-to-digital conversion (ADC) can be rewritten in the discrete time domain as following:

$$R_{IF}(k) = A \cdot cos((\omega_{IF} + \omega_D)T_s k + \varphi)\, y(T_s k - \tau) d(T_s k - \tau) + n(k) \qquad (4)$$

where T_s is the sampling time interval, and $t = T_s k$; $\frac{\omega_{IF}}{2\pi} = f_{IF}$ and $\frac{\omega_D}{2\pi} = f_D$ represent the intermediate frequency and Doppler frequency, respectively; $n(k)$ is the corresponding noise at intermediate frequency. In the tracking loop, the local replica signal is generated. Despite the navigation data, the local replica can be given by:

$$\hat{R}_{IF}(k) = cos((\omega_{IF} + \widehat{\omega}_D)T_s k + \hat{\varphi})\, y(T_s k - \hat{\tau}) \qquad (5)$$

where $\hat{\varphi}, \hat{\tau}, \widehat{\omega}_D$ are the estimations of the carrier phase, code delay and Doppler frequency, respectively.

In the phase lock loop (PLL), the discriminator block calculates the estimated carrier phase error and the numerically-controlled oscillator (NCO) will adjust the frequency of the local replica correspondingly. The NCO carrier phase is defined as:

$$\hat{\varphi}_{NCO}(k) = 2\pi\left(f_{IF} + \hat{f}_D\right)T_s k + \hat{\varphi}(k) \tag{6}$$

If the signal is steadily tracked, the PLL drives estimated carrier phase error to zero.

$$\hat{\varphi}_{NCO}(k) - 2\pi(f_{IF} + f_D)T_s k - \varphi(k) \to 0 \tag{7}$$

The signal carrier phase measurement is the difference between the NCO carrier phase and the nominal increase. Therefore, the carrier phase of the received signal can be expressed as Eq. (8) in Teunissen and Montenbruck (2017).

$$\varphi(k) = \hat{\varphi}_{NCO}(k) - 2\pi f_{IF} T_s k \tag{8}$$

In the processing of the software receiver, it can be achieved by the integration of the Doppler frequency over time. Then the propagation path difference (Δd) between the direct and reflected signal is given by:

$$\Delta d = (\varphi_d - \varphi_r)\lambda/2\pi = N\lambda + \varphi_\Delta \lambda/2\pi \tag{9}$$

Where, λ is the wavelength of GPS L1 signal, N is the integer number of wavelength, and φ_Δ is the fraction part of the carrier phase difference. If the environment is fixed, the propagation path difference will be a function that only depends on the satellite movement. When the observed target moves, there will be additional propagation path occurring and resulting in the carrier phase difference deviating from the original track.

To reveal the relationship between the deformation and the carrier phase difference of signals, a geometrical model has been developed to count for the carrier phase changes due to the movement of satellites. The propagation path simulation of the direct and reflected signal is shown in figure 2. In the certain scenario, the satellite elevation angle (θ) and azimuth angle (α_s) can be calculated based on the satellite ephemeris data and the antenna position. The slope surface tilt angle (γ), azimuth angle (α_r) and the vertical distance between the antenna and the slope surface (d) can also be retrieved.

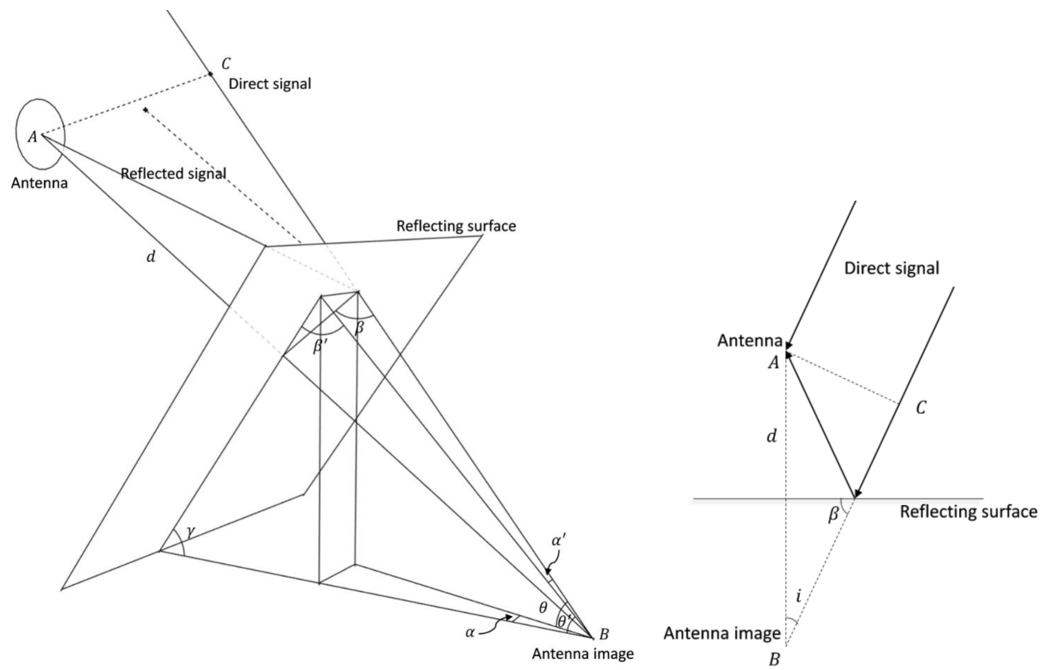

Figure 2. The signal reflection model

In this figure 2, the angle β is equal to the complementary of the signal incident angle i and can be regarded as the equivalent elevation angle. And angle $\alpha = \alpha_s - \alpha_r$, is the difference between the azimuth angle of satellite and of the slope surface. And the angle θ' and β' are the projections of satellite elevation angle θ and equivalent elevation angle β on the front surfaces, respectively. The front surface is perpendicular to the ground and the slope surface. For easy understanding, the plane ABC in the 3D model is highlighted on the right of figure 2, and the propagation path difference is shown as BC. Hence, for the geometrical simulation, the propagation path difference (Δd) between the direct and reflected signal is given by:

$$\begin{cases} \Delta d = 2d\, sin\, \beta = 2d\, cos\, i \\ sin\, \beta = sin\, \beta'\, cos\, \alpha' \\ \beta' = \pi - \theta' - \gamma \\ tan\, \alpha' = tan\, \alpha\, cos\, \theta' \\ tan\, \theta = tan\, \theta'\, cos\, \alpha \\ \alpha = \alpha_s - \alpha_r \end{cases} \tag{10}$$

This geometry model transfers the satellite elevation angle to the incident angle with respect to the reflecting surface, which can solve the complexity of the forward or backward scattering problem. There are two factors that influence the propagation path difference: the vertical distance between the antenna and the slope surface (d), and the equivalent elevation angle (β). The equivalent elevation angle β will change time to time due to the satellite movement. Hence, the propagation path difference (Δd) will not be a constant even there is no slope deformation occurring during the observation.

Assuming the direct and reflected signal have been steadily tracked during observation, for arbitrary moments before and after the deformation occurring, the following equations hold:

$$\begin{cases} \Delta d = 2d\,sin\,\beta = N\lambda + \varphi_{\Delta}\lambda/2\pi \\ \Delta d' = 2(d + d_{def})\,sin\,\beta' = N\lambda + \varphi'_{\Delta}\lambda/2\pi \end{cases} \tag{11}$$

where, d_{def} is the deformation of the reflecting surface, along the normal direction; β and β' are the equivalent elevation angle before and after the deformation, respectively. And N is the carrier phase ambiguity. Assuming no circle slip occurred, due to the continuous observation, the ambiguity is same before and after the deformation.

Therefore, the changes of the carrier phase difference φ''_{Δ} should be:

$$\frac{\varphi''_{\Delta}\lambda}{2\pi} = \frac{(\varphi_{\Delta} - \varphi'_{\Delta})\lambda}{2\pi} = 2d(sin\,\beta - sin\,\beta') - 2d\,sin\,\beta'\,d_{def} \tag{12}$$

Then the deformation value of the reflecting surface can be calculated by:

$$d_{def} = \frac{2d(sin\,\beta - sin\,\beta') - \dfrac{\varphi''_{\Delta}\lambda}{2\pi}}{2\,sin\,\beta'} \tag{13}$$

where, the term $2d(sin\,\beta - sin\,\beta')$ represents the carrier phase difference caused only by the satellite movement, which can be eliminated by the geometry model. Notice here the d_{def} represents the deformation along the normal direction of the object surface.

Finally, the workflow of the slope deformation monitoring using GNSS-R can be given as figure 3.

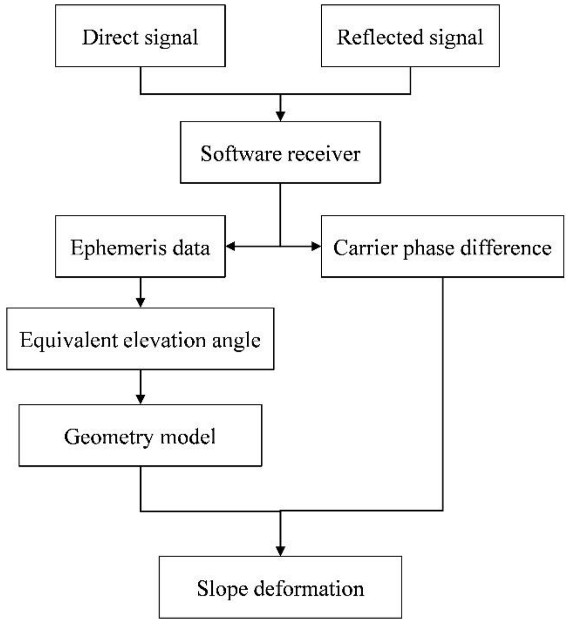

Figure 3. The workflow of slope deformation monitoring using GNSS-R

GNSS-R receiver

To ensure the accurate results of carrier phase difference, the direct and reflected signals are required to be strictly synchronized. A custom-made dual-channel GPS/Galileo L1 radio frequency recorder was employed for signal collection. This front-end receiver provides two parallel channels, which are synchronized by one oven-controlled crystal oscillator (OCXO) to eliminate the receiver clock error. Each channel can be considered as an independent front-end, which connects to a GNSS antenna for the radio frequency (RF) signal collection. The structure of the front-end is shown in figure 4.

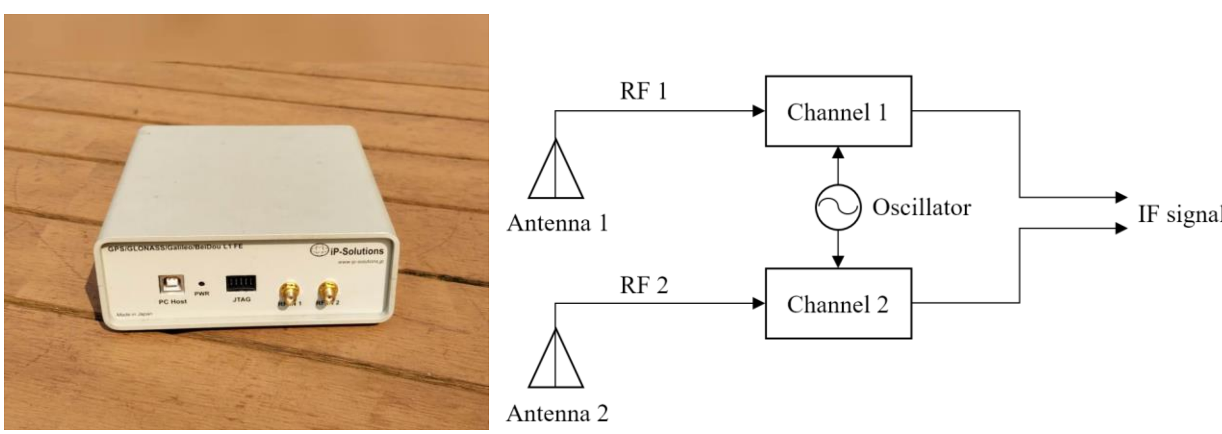

Figure 4. The iP-solutions GNSS-R front-end and its structure

The collected RF signal is down-converted to the intermediate frequency (IF) and then digitized and sampled. The device outputs 2-bit real-time data from each front-end channel. The RF recording software was installed on the host computer to manage the collection procedure. The IF stream data is delivered to the connected computer and stored on hard disk. The other specifications of the front-end are shown in table 1:

Antenna connector	SMA
Bandwidth (MHz)	4
Sampling rate (MHz)	16.368
Intermediate frequency (MHz)	4.092
Resolution	2 bits

Table 1. Specifications of iP-solutions front-end

A software receiver has been developed to process the synchronized dual-channel baseband signal. The normal IF signal processing flow is applied to each channel. There are two independent baseband signal processing modules. And the tracking results like carrier phase, pseudorange and Doppler frequency of each channel will be outputted. For further analysis, the pseudorange difference, carrier phase difference and Doppler frequency difference are also calculated. In the case of continuously monitoring, the change of the carrier phase difference between the direct and reflected signal is the most interested. The structure of the software receiver is shown in figure 5.

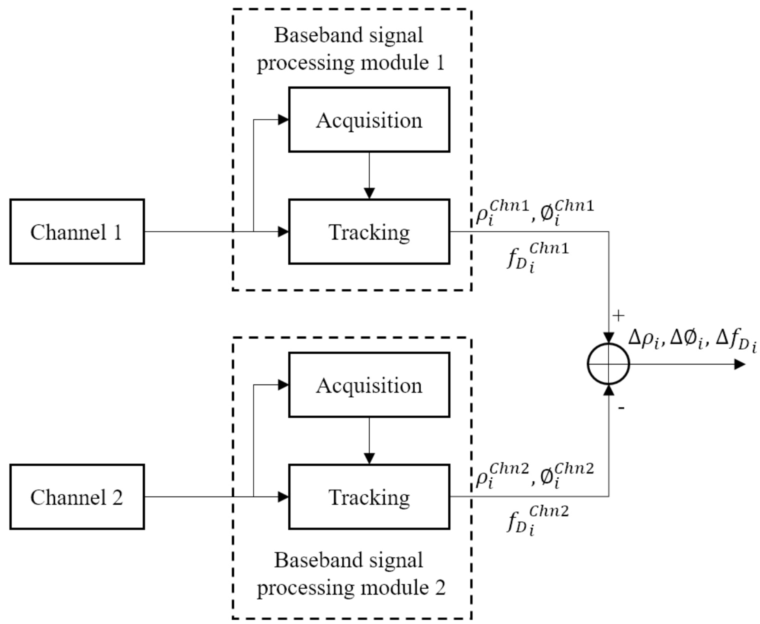

Figure 5. Structure of independent baseband signal processing

Experiment implementation and results

Two experiments have been designed and implemented to verify the proposed method for deformation monitoring. Because it is difficult to find a slope in the progress of deformation for experiment, different methods have been used to simulate deformation. The first experiment has been conducted with a controllable reflector, then the deformation estimation accuracy can be evaluated by comparing with the true movement of the reflector. To examine the feasibility of this method, the performance under long distance scenario was tested in the second experiment. In this case, we placed the GNSS-R Receiver 350 m away from a slope. Then antenna of GNSS-R receiver was moved back and forth to simulate the deformation.

1) Experiment with a reflector

An experiment has been designed to simulate the environment of slope deformation and verify this algorithm. An aluminum-foiled reflector with a dimension of 2.0*1.5 meters was made to mimic the reflecting surface. A man-made reflector can ensure that the reflecting surface will have movement occurring during observation. The sitting-out area in Ho Man Tin, Hong Kong, was selected as the experiment location, as shown in figure 6. This place has the open surrounding environment and a slope next to it. The slope tilt angle is about 42 degrees, and azimuth angle is about 190 degrees from north. The reflector was placed on the slope as a controllable reflecting surface. The slope distance between the antenna and the reflector was about 25 meters. An RHCP antenna was installed on the tripod facing zenith to collect the direct signal, and an LHCP antenna was facing to the slope to collect the reflected signal. Each signal collection lasts for 1 minute and was saved as one dataset. To simulate the slope deformation, the reflector was moved horizontally towards the antenna for 2 cm while signal collection.

Figure 6. The environment of experiment location at Ho Man Tin sitting-out area.

The GPS signals of PRN 15 and PRN 29 have been received simultaneously by both channels during the experiment. The carrier-to-noise ratio (CN_0) have been processed as shown in figure 7, which are very similar to GNSS direct signals. Depending on the position of GPS satellite, the specular point position on the slope varies correspondingly. The GNSS-SAR images have been first processed to verify the specular point position (Zheng et al., 2017). The image represents the power of the reflected signal from corresponding areas. The highlighted zone means the area which reflects higher power, and in this case, it indicates the position of the specular point.

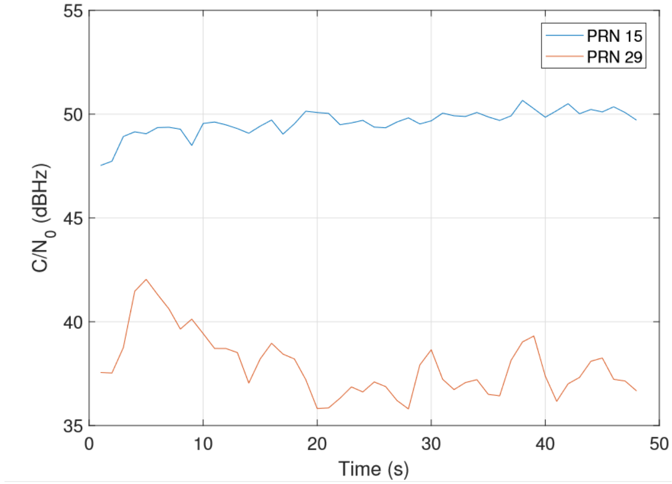

Figure 7. The CN0 of PRN 15 and PRN 29.

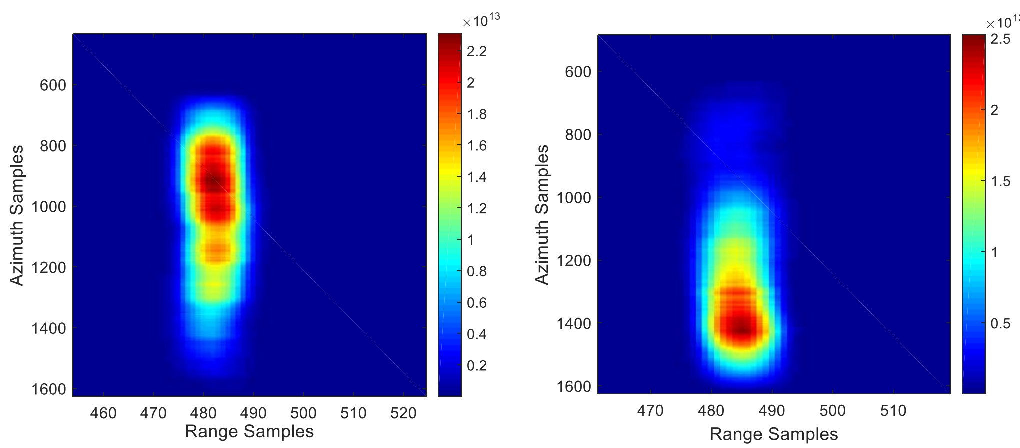

Figure 8. The GNSS-SAR images of PRN 15 (left) and PRN 29 (right)

As shown in figure 8, the range sample represents the distance along the range direction, which is the direction from the antenna to the reflector; and the azimuth sample represents the distance along the azimuth direction, which is along the slope and perpendicular to the range direction. The GNSS-SAR image resolution of range direction is relatively lower (18 m) due to the low chip rate of C/A code. Whereas the azimuth resolution reaches centimeters level for each pixel at the distance of 25 meters, which is considerably higher compared with the range resolution. The details of conducting the GNSS-SAR image can refer to the previous work (Zheng et al., 2017). In range direction, the positions of specular points corresponding to the signal of PRN 29 and PRN 15 are indistinguishable from the GNSS-SAR image. However, in the azimuth direction, it is obvious that the specular points are at different positions.

The received signals of both channels have been fed into the software receiver for signal acquisition and tracking. The carrier phase difference between the direct and reflected signal has been processed for both PRN15 and PRN29, as shown in blue lines figure 9. The phase corrections for the satellite movements for the two satellites are also plotted in Figure 9 (red lines).

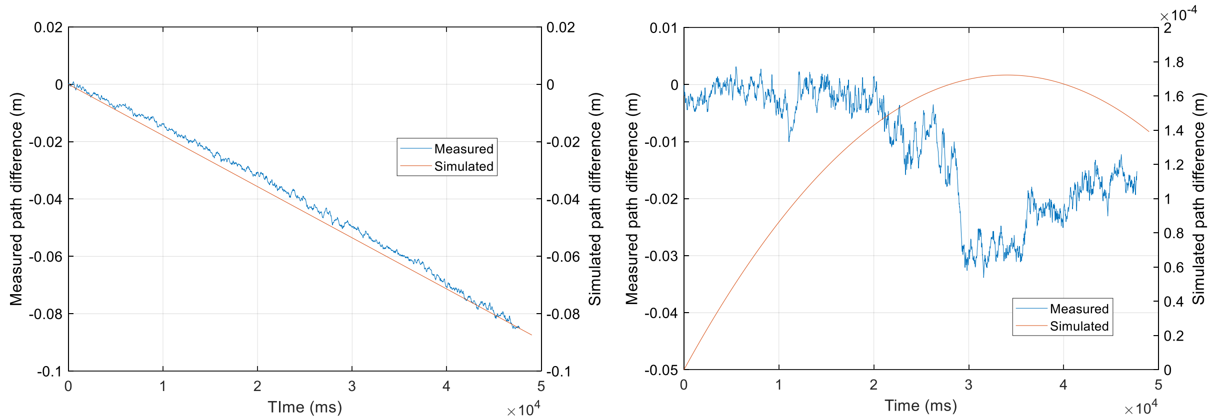

Figure 9. The carrier phase difference between direct and reflected signal of PRN 15 (left) and PRN 29 (right).

The deformation of the reflecting points can then be obtained by removing the carrier phase changes caused by the satellite movements, as shown in figure 10.

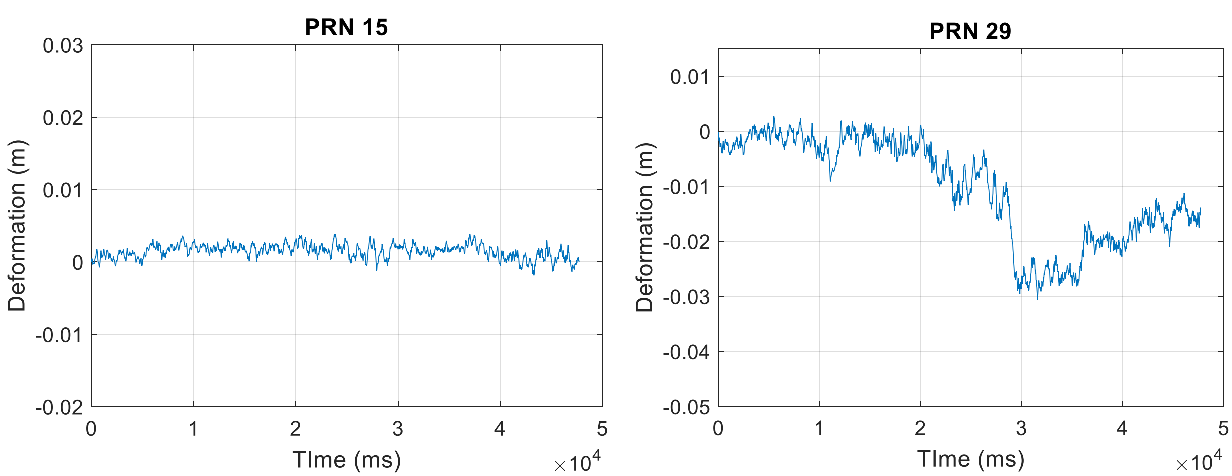

Figure 10. The deformation value of reflecting surface of PRN 15 (left) and PRN 29 (right).

In figure 10 it can be seen that the deformation outputted of PRN 15 shows millimeter level changes during that time. Judging by the GNSS-SAR image and the outputted carrier phase difference, the reflected signal of PRN 15 is not coming from the reflector but from the slope surface. The deformation results fit nicely to zero with the acceptable noise level (mean of 0.15 cm and Std. of 0.95 mm).

From the results of PRN 29, a distinct leap shows at about 30 seconds, which represents the movement of the reflector. The noise of the results of PRN 29 is noticeable larger compared with PRN 15, which might be caused by the vibration of the aluminum foil. To confirm the stable status before and after the movement and to see when the movement ends, the standard deviations of deformation value are calculated, as well as the mean values of the two stable statuses to analyze the precision of the results, as shown in table 2.

	Std. (mm)	Mean (cm)
Before movement	1.91	-0.17
After movement	2.02	-1.73

Table 2. The analysis of the deformation monitoring results

The mean value difference is -1.56 cm, which represents the slope deformation along the normal direction, and the negative value represents that the reflecting surface was deforming towards the antenna. In this case, the reflector was moved horizontally of 2 cm (that is 1.34 cm on the normal direction with tilt angle of 42 degrees). To verify the monitoring stability, more datasets have been collected and the deformation results have been processed. The corresponding deformation in normal direction have been listed on table 3, as well as the error with respect to the movement truth of 1.34 cm. The mean error of all monitoring results is 0.37 cm, and the RMSE is 0.48. The results confirm the precision of sub-centimeter level can be achieved by this deformation monitoring method.

	Deformation in normal direction (cm)	Error (cm)
Dataset 1	-1.56	0.22
Dataset 2	-1.21	-0.13
Dataset 3	-1.58	0.24
Dataset 4	-1.85	0.51
Dataset 5	-2.22	0.88
Dataset 6	-1.83	0.49

Table 3. The deformation monitoring results.

In this experiment, the applying of the reflector was only to create an artificial deformation scenario to verify the precision of the proposed method. If the signal quality from the slope surface and the reflector were at same level, then the precision achieved above could also apply to the situation without the reflector. In the results above, the signal strength of PRN 15 is higher and more stable than which from PRN 29, and the tracking results of PRN 15 also shows lesser noise. Yet the satisfied precision could also be achieved by PRN 29. This can provide the evidence that the proposed method could be used for deformation monitoring and the corresponding precision can be achieved.

2) Experiment of long distance

Another experiment has been conducted to verify the performance of this algorithm under long distance scenario. A slope with cement solidified surface and trees on it has been chosen as the target, as shown in figure 11. The RHCP and LHCP antennas and receiver have been deployed on Lantau Link Viewing Platform, with about 350 meters to the slope surface. The tilt angle of the slope surface is about 65 degrees, and azimuth angle is about 270 degrees from north. In this experiment, the reflector was not employed. However, the reflected antenna was moved forward and backward to simulate the deformation of the slope surface. The movement of the antenna was also 2 cm horizontally during the observation.

Figure 11. The experiment environment of long distance

The GPS satellite PRN 2 and PRN 6 have been steadily tracked during observation, the CN_0 have been processed as shown in figure 12. Due to the longer distance, the signal strength of received signal is weaker and unstable. The GNSS-SAR image have been processed to verify the position of the specular point, as shown in figure 13. In the range direction, it shows the extra propagation path between the direct and reflected signal, which confirms the rough distance between the antenna and the slope surface by considering the equivalent elevation angle. Then the signals have been processed by the software receiver, the measured and the simulated carrier phase difference have been achieved, as shown in figure 14. The signal strength of PRN 2 is higher than PRN 6 and the corresponding carrier phase difference shows less noise. Comparing with the close-range experiment, the carrier phase difference changes faster due to the longer distance. The tracking status in the beginning of PRN 2 is not steady, and a circle slip occurred as a result. For easily demonstrate, the outputted carrier phase difference was manually adjusted to around zero by subtracting a constant.

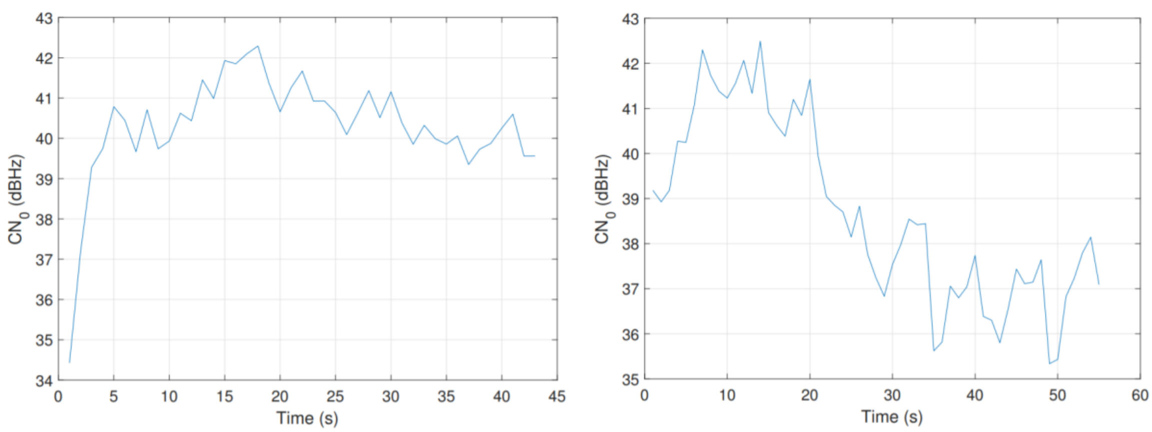

Figure 12. CN_0 of PRN 2 (left) and PRN 6 (right).

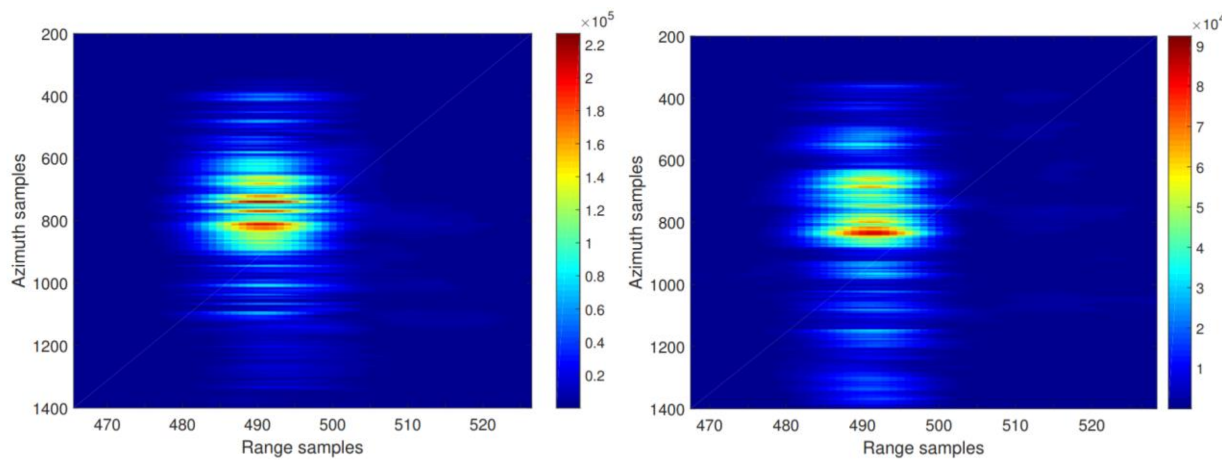

Figure 13. GNSS-SAR images of PRN 2 (left) and PRN 6 (right).

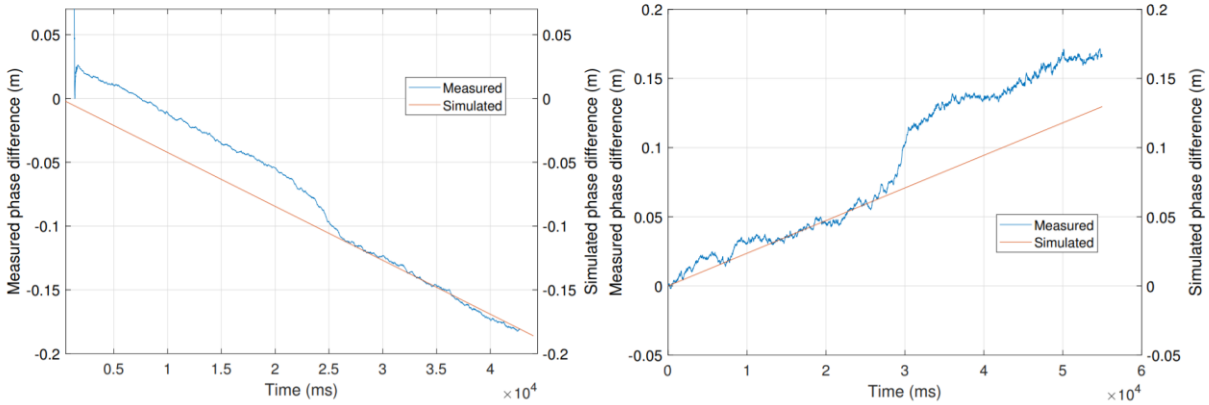

Figure 14. Measured and simulated carrier phase difference of PRN 2 (left) and PRN 6 (right).

Finally, the deformation along the normal direction can be calculated and shown in figure 15. And the mean values of two stable statuses have been calculated to verify the precision in this scenario, as listed in table 4.

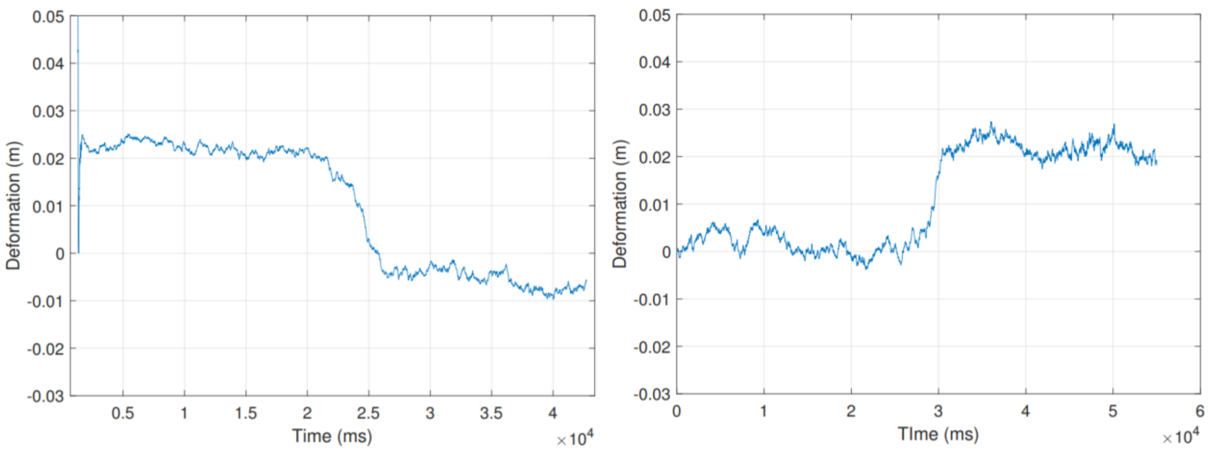

Figure 15. Deformation results of PRN 2 (left) and PRN 6 (right).

	Mean before movement (cm)	Mean after movement (cm)	Deformation (cm)
PRN 2	2.22	-0.53	-2.75
PRN 6	2.19	0.15	2.04

Table 4. The deformation results of PRN 2 and PRN 6.

The deformation results of PRN 2 indicate the forward movement of the antenna, while the results of PRN 6 indicate the backward movement. Considering the tilt angle of the slope surface, the deformation along the normal direction should be 1.81cm, then the monitoring error of PRN 2 and PRN 6 should be 0.94 and 0.23 cm, respectively.

This experiment demonstrated the performance of this algorithm under long distance scenario. Instead of using the reflector as a controllable reflecting surface, the antenna was moved back and forth to simulate the movement of the slope. The signals received show lower strength and higher noise, as well as the tracking status, compared with the previous experiment. And the sub-centimeter level accuracy could also be achieved.

Conclusions

In this paper, we have discussed the theory of using GNSS-R technology for deformation monitoring and demonstrated the potential applications of the proposed theory. A GPS software receiver is developed for the purpose. Carrier phase differences between the direct and reflected GPS signals are estimated using GPS IF data collected by the GPS software receiver. A geometrical model is used to correct the carrier phase difference due to the motion of GPS satellites. Experiments are designed to evaluate the deformation monitoring performance in aspects of accuracy, stability and detectability in both close- and long-range scenario. The results show that the deformation measurement accuracy of sub-centimeter can be achieved.

The proposed method of using GNSS-R for deformation monitoring requires continuous observation, and because of the data size, the observation duration is limited by the equipment. This method is suitable for relatively short-term monitoring, especially in the case of emergency. The long-term monitoring needs further study in terms of discontinuous observation and small data size. The multipath is a main error source. The direct signal multipath can be significantly reduced by using the choking-ring antenna, or by adjusting the antenna direction towards the satellite, based on the geometry of observation. However, the reflected signal multipath represents there are more than one objects that can reflect signals to the antenna. In this situation, it needs further study because the reflected signal is the combination of multiple signals as well as the carrier phase. The alternative option of solving this problem is to use directional antenna (antenna with narrower half-power beamwidth), which can be set to point to proper direction for target monitoring. Also, with higher antenna forward gain, the maximum distance could be longer, and the application scenario could be expanded significantly. Also, in this study, we collect GPS IF data and process them in a post-processing method. Real-time processing algorithms need to be implemented for real operation. And the other satellite system like Galileo, GLONASS and BD system can also be used in the future work for more opportunities of observation.

References

Cardellach, E., Rius, A., Martín-Neira, M., Fabra, F., Nogues-Correig, O., Ribo, S., . . . D'Addio, S. (2014). Consolidating the precision of interferometric GNSS-R ocean altimetry using airborne experimental data. *Ieee Transactions on Geoscience and Remote Sensing, 52*(8), 4992-5004.

Egido, A., Ruffini, G., Caparrini, M., Martin, C., Farres, E., & Banque, X. (2008). Soil moisture monitorization using GNSS reflected signals. *arXiv preprint arXiv:0805.1881*.

Erol, S., Erol, B., & Ayan, T. (2004). *A general review of the deformation monitoring techniques and a case study: Analyzing deformations using GPS/leveling.* Paper presented at the XXth ISPRS Congress.

Ferrazzoli, P., Guerriero, L., Pierdicca, N., & Rahmoune, R. (2011). Forest biomass monitoring with GNSS-R: Theoretical simulations. *Advances in space research, 47*(10), 1823-1832. doi:https://doi.org/10.1016/j.asr.2010.04.025

Hu, C., Benson, C., Rizos, C., & Qiao, L. (2017). Single-Pass Sub-Meter Space-Based GNSS-R Ice Altimetry: Results From TDS-1. *Ieee Journal of Selected Topics in Applied Earth Observations and Remote Sensing*.

Jacobson, M. D. (2008). Dielectric-covered ground reflectors in GPS multipath reception—Theory and measurement. *Geoscience and Remote Sensing Letters, IEEE, 5*(3), 396-399.

Larson, K. M., Braun, J. J., Small, E. E., Zavorotny, V. U., Gutmann, E. D., & Bilich, A. L. (2010). GPS multipath and its relation to near-surface soil moisture content. IEEE Journal of Selected Topics in Applied Earth Observations and Remote Sensing, 3(1), 91-99. Li, W., Cardellach, E., Fabra, F., Rius, A., Ribó, S., & Martín‐Neira, M. (2017). First Spaceborne Phase Altimetry over Sea Ice Using TechDemoSat‐1 GNSS‐R Signals. *Geophysical Research Letters*.

Lowe, S. T., Zuffada, C., Chao, Y., Kroger, P., Young, L. E., & LaBrecque, J. L. (2002). 5-cm-Precision aircraft ocean altimetry using GPS reflections. *Geophysical Research Letters, 29*(10).

Martin-Neira, M. (1993). A passive reflectometry and interferometry system (PARIS): Application to ocean altimetry. *ESA journal, 17*, 331-355.

Park, H., Lee, H., Adeli, H., Lee, I., 2007. A new approach for health monitoring of structures: terrestrial laser scanning. Computer-Aided Civil and Infrastructure Engineering 22 (1), 19-30.

Rius, A., Nogués-Correig, O., Ribó, S., Cardellach, E., Oliveras, S., Valencia, E., . . . van der Marel, H. (2012). Altimetry with GNSS-R interferometry: first proof of concept experiment. *GPS solutions, 16*(2), 231-241.

Rivas, M. B., & Martin-Neira, M. (2006). Coherent GPS reflections from the sea surface. *Ieee Geoscience and Remote Sensing Letters, 3*(1), 28-31.

Ruffini, n. G., Soulat, F., Caparrini, M., Germain, O., & Martín‐Neira, M. (2004). The Eddy Experiment: Accurate GNSS‐R ocean altimetry from low altitude aircraft. *Geophysical Research Letters, 31*(12).

Semmling, M., Beyerle, G., Beckheinrich, J., Ge, M., & Wickert, J. (2014). *Airborne GNSS reflectometry using crossover reference points for carrier phase altimetry*. Paper presented at the Geoscience and Remote Sensing Symposium (IGARSS), 2014 IEEE International.

Soulat, F., Caparrini, M., Germain, O., Lopez‐Dekker, P., Taani, M., & Ruffini, G. (2004). Sea state monitoring using coastal GNSS‐R. *Geophysical Research Letters, 31*(21).

Teunissen, P., & Montenbruck, O. (2017). Signal processing. In J. Won & T. Pany (Eds.), *Springer handbook of global navigation satellite systems*. (pp. 401-442). Springer.

Treuhaft, R. N., Lowe, S. T., Zuffada, C., & Chao, Y. (2001). 2‐cm GPS altimetry over Crater Lake. *Geophysical Research Letters, 28*(23), 4343-4346.

Zheng, Y., Yang, Y., & Chen, W. (2017). Enhanced GNSS-SAR Range-Doppler Algorithm for The Target Detection of Weak Reflected Signals: An Experimental Study. *Journal of Aeronautics, Astronautics and Aviation, 49*(2), 83-92.